ANALYSIS OF CRYSTALLITE SIZE CHANGES IN AN OXIDE LAYER FORMED ON 13CrMo4-5 STEEL USED IN THE POWER INDUSTRY

Monika GWOŹDZIK [1]

[1]*Czestochowa University of Technology, Faculty of Production Engineering and Materials Technology, Institute of Materials Engineering, Czestochowa, Poland, EU*
gwozdzik.monika@wip.pcz.pl

Abstract

The paper presents results of studies on the crystallite sizes of oxide layer formed during a long-term operation on 13CrMo4-5 steel at an elevated temperature (T=470°C, t=190,000h). This value was determined by a method based on analysis of the diffraction line profile, according to a Scherrer formula. The oxide layer was studied on a surface and a cross-section at the outer and inner site on the pipe. X-ray studies were carried out on the surface of a tube, then the layer's surface was polished and the diffraction measurements repeated to reveal differences in the originated oxides layer.

Keywords: 13CrMo4-5 steel, XRD diffraction, crystallite sizes

1. INTRODUCTION

The material engineering is a field of science enjoying the interest of many centers in the world [1-10]. More and more research are devoted to surface engineering [3, 5, 9, 11, 12], especially the oxidation of materials applicable in the energy industry [11-26]. Boilers, the most troublesome components of electric power, chemical and processing plants generate high costs in unscheduled shutdowns, repairs and power replacement. Every occurrence of ruptured tubes leads to emergency shutdown of the entire plant [8]. In paper [8] the research evaluation included non-contact wall thickness measurement with EMAT technology plus internal oxide layer measurement with specialized ultrasonics. In paper [27] the authors showed that the scale which formed on the 2.25 % Cr-1 % Mo steel tube exposed in steam at 550 °C to 625 °C for 300 h to 10,000 h comprises with the outer scale composed of Fe_3O_4 with a slight amount of Fe_2O_3 and the inner scale composed of $(Fe, Cr)_3O_4$. In paper [28] the high temperature corrosion behavior of the boiler steels 13CrMo4-5 (1.7335), P91 (1.4903) and 1.4541 has been investigated during short-term test runs (~500 h) at a biomass fired grate furnace combined with a drop tube. General trends determined by the variation of these temperatures were similar for all boiler steels: the corrosion rate increased with increasing flue gas temperature and also with increasing probe surface temperature.

2. MATERIALS AND EXPERIMENTAL METHODS

The material studied comprised specimens of 13CrMo4-5 steel operated at the temperature of 470 °C during 190.000 h. The chemical compositions and operating parameters of steel are given in **Table 1**.

Table 1 Chemical composition of examined steel and acc. EN 10028-2 [29]

Chemical composition, wt. %							
Acc.	C	Si	Mn	P	S	Cr	Mo
Analysis	0.15	0.24	0.50	0.022	0.009	0.94	0.51
EN [29]	0.08-0.18	Max. 0.35	0.40-1.00	Max. 0.025	Max. 0.010	0.70-1.15	0.40-0.60

The analysis of the chemical composition of the steel was carried out using spark emission spectroscopy on a Spectrolab spectrometer. The oxide layer was studied at the outer site (the flowing gas side) and at the inner site (the flowing steam side) on the pipe (**Figure 1**).

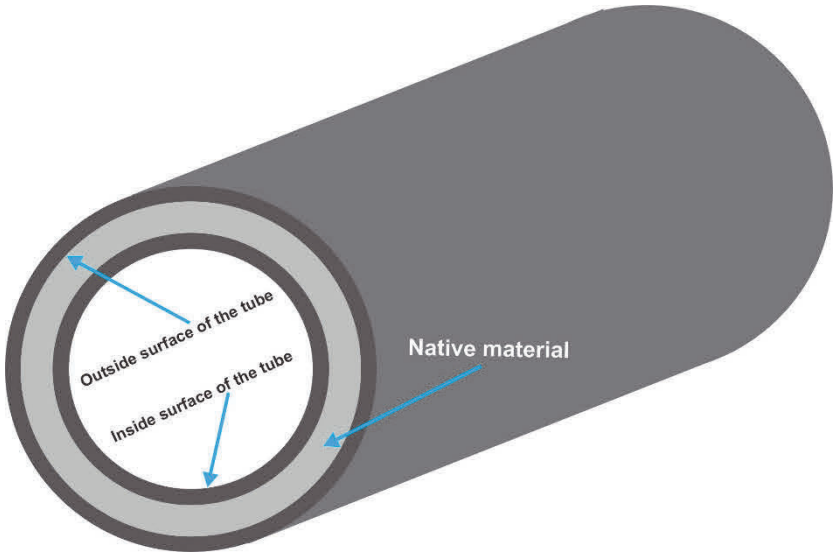

Figure 1 Place of samples taking for tests

Thorough examinations of the oxide layer carried out on the outer surface of tube wall comprised:

- Microscopic examination of the oxide layer were performed using a Jeol JSM-6610LV scanning electron microscope (SEM),
- chemical composition analysis of deposits/oxides using a Jeol JSM-6610LV scanning electron microscope (SEM) working with an Oxford EDS electron microprobe X-ray analyser,
- X-ray (XRD) measurements (studying the phase composition, crystallite sizes); the layer was subject to measurements using a Seifert 3003T/T X-ray diffractometer and the radiation originating from a tube with a cobalt anode (λ_{Co} = 0.17902 nm). X-ray studies were performed, comprising measurements in a symmetric Bragg-Brentano geometry (XRD). Computer software and the PDF4+2009 crystallographic database were used for the phase identification.

Based on the width and the position of the main coat and substrate reflections, the size of the crystallites was determined using the Scherrer formula (1) [15, 16, 21, 30]:

$$D_{hkl} = \frac{k \cdot \lambda}{\beta \cdot \cos\Theta} \tag{1}$$

where: D_{hkl} - crystallite size in the direction normal to (hkl), nm; k - constant (~1); λ - radiation wavelength, nm; β - reflection width depending on the crystallite size, rad; θ - Bragg angle, rad.

X-ray studies were carried out on the surface, and then the layer surface was polished down and the diffraction measurements were performed again to determine individual oxide layers. The size of the D_{hkl} crystallites size was determined for the reflections originating from the planes (104) for Fe_2O_3 and (311) for Fe_3O_4, which are occurring at angles of 38.7464° and 40.8998°, respectively (according to the catalog card ICDD PDF 01-079-0007 and ICDD PDF 01-089-0951). X-ray measurements were performed at different depths of the oxide layer. After removal of the sediment layer, the X-ray measurements were carried out, then, the oxide layer was removed (5 μm) cyclically, each time making XRD measurements:

- from steam side, the oxide layer was removed every 5 μm in 10 cycles,
- from exhaust side, the oxide layer was removed every 5 μm in 16 cycles.

3. RESULTS OF EXAMINATION

The obtained results of studies have shown that on the inside of a tube wall, directly on the steam flow side, there is a layer of hematite (Fe_2O_3), under which a layer of magnetite (Fe_3O_4) exists. On the inside, directly on the steel side, apart from iron, the oxide layer is enriched in addition of such elements as Cr, Mn, Mo, and Si, depending on the chemical composition of studied steel (**Figure 2**). Maps of elements distribution have shown that chromium exists in 2/3 of the layer oxide thickness, moving from the substrate (steel). The total thickness of oxide layer on the inside in the widest place was 57.58 μm, which was presented in paper [22]. The oxides/deposits layer, which originated on the outside of the tube wall, substantially differs from the oxide layer, which formed on the inside. On this surface, directly on the flue gas inflow side, on the surface itself and moving inside the layer to a depth of 74 μm, there exist compounds based on Ca, As, K, Al, Na, and Zn, which was shown in paper [22]. Below this layer Fe_2O_3 exists alternately with such compounds as: As_2O_3, $KAlSi_2O_6$, Na_6ZnO_4, and ZnO_2. Fe_3O_4 appears moving deeper inside the layer (**Figure 3**, **Figure 4**).

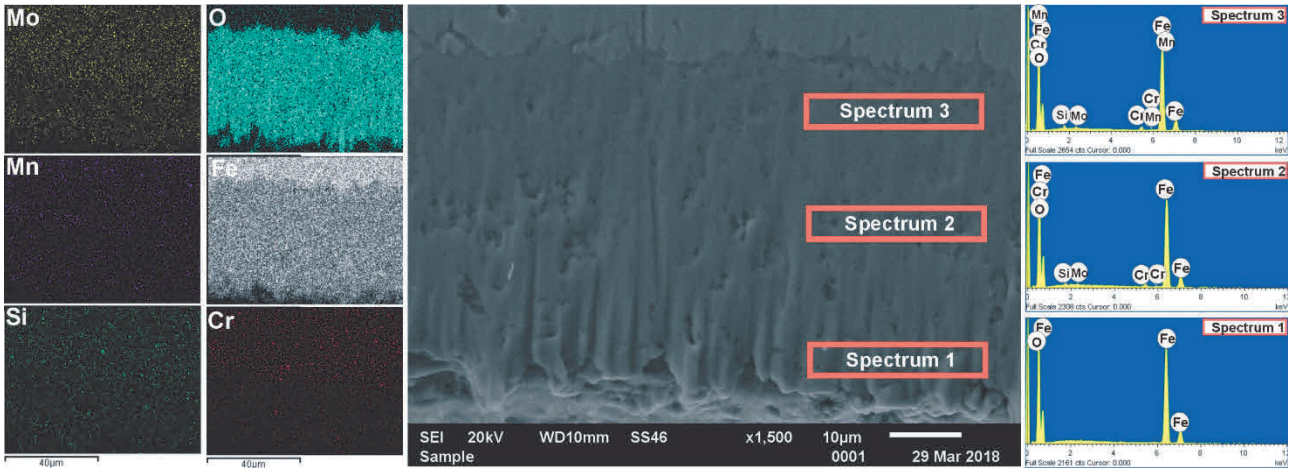

Figure 2 SEM images of the steel samples, EDS analysis and maps of the distribution of elements, inner site on the pipe

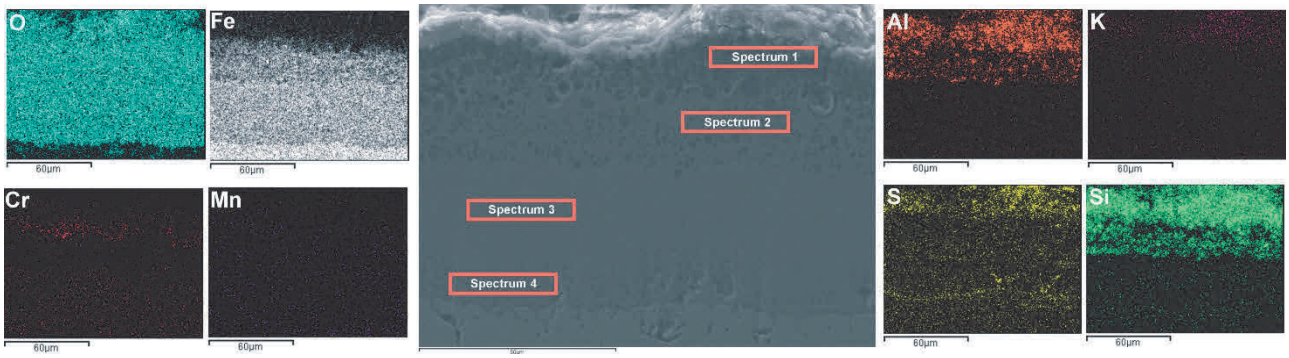

Figure 3 SEM images of the steel samples, the maps of the distribution of elements, outer site on the pipe

The obtained results of crystallites measurement have shown that in the case of the oxide layer formed on the steam flow side, D_{hkl} for hematite at a depth of 10 μm from the surface reaches the highest values (**Figure 5A**). Moving deeper inside the layer, the crystallite sizes successively diminish. On the outside of the tube wall, D_{hkl} for hematite at a depth of 60 to 65 μm was 19.87 nm and 21.76 nm respectively (**Figure 5B**). At a depth of 70 to 75 μm, the size of hematite crystallites suddenly increased to 37.79 nm and 46.23nm respectively, and then this parameter has slightly decrease approx. 10 units at a depth up to 80 μm; after this

was slightly grown (at a depth of 85 to 90 μm) and the next this parameter value was going down after further successive removal of the layer.

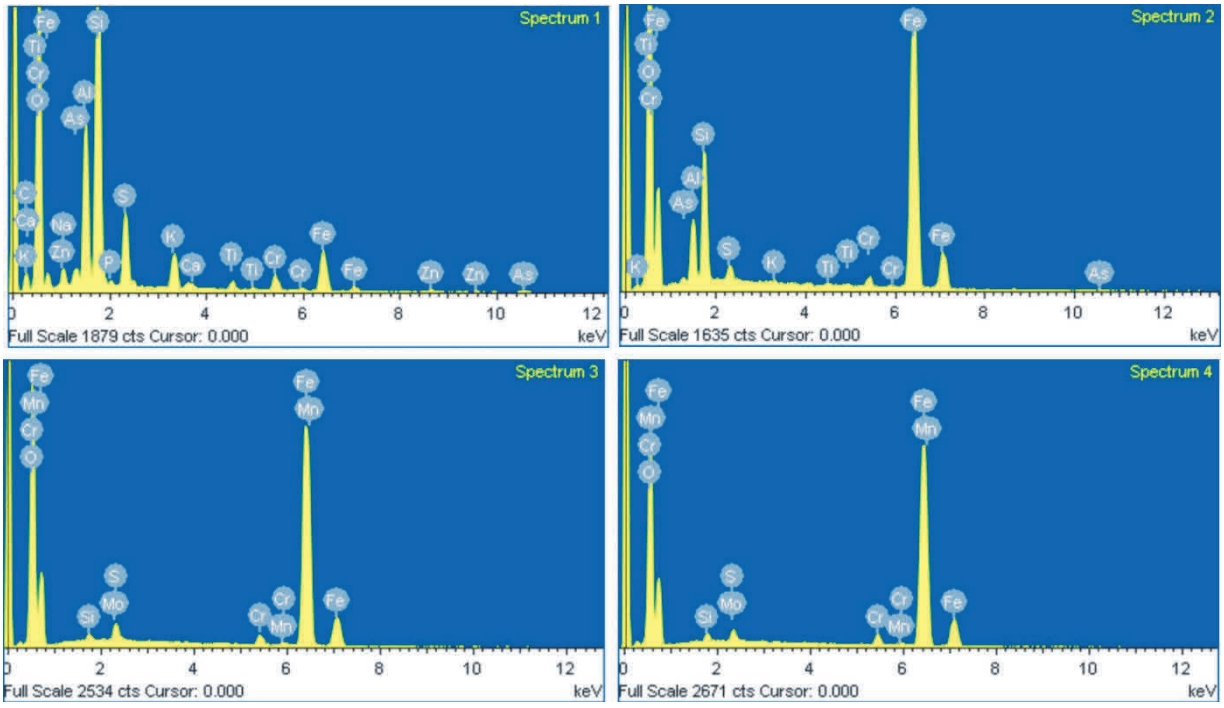

Figure 4 EDS analysis of elements, outer site on the pipe

For magnetite on the inside D_{hkl} directly under the hematite layer amounts to approximately 28,51 nm, and then this parameter slightly grows at a depth of 15 to 25 μm, which is followed by a linear decline (**Figure 5C**). In the case of the tube wall outside, the crystallite sizes gradually increase to a depth of 95 μm, and then D_{hkl} slightly declines to a depth of 110 μm. At a depth of 115 to 120 μm another increase in this parameter was observed. Instead, once 120 μm is exceeded, the value of this parameter substantially goes down (**Figure 5D**).

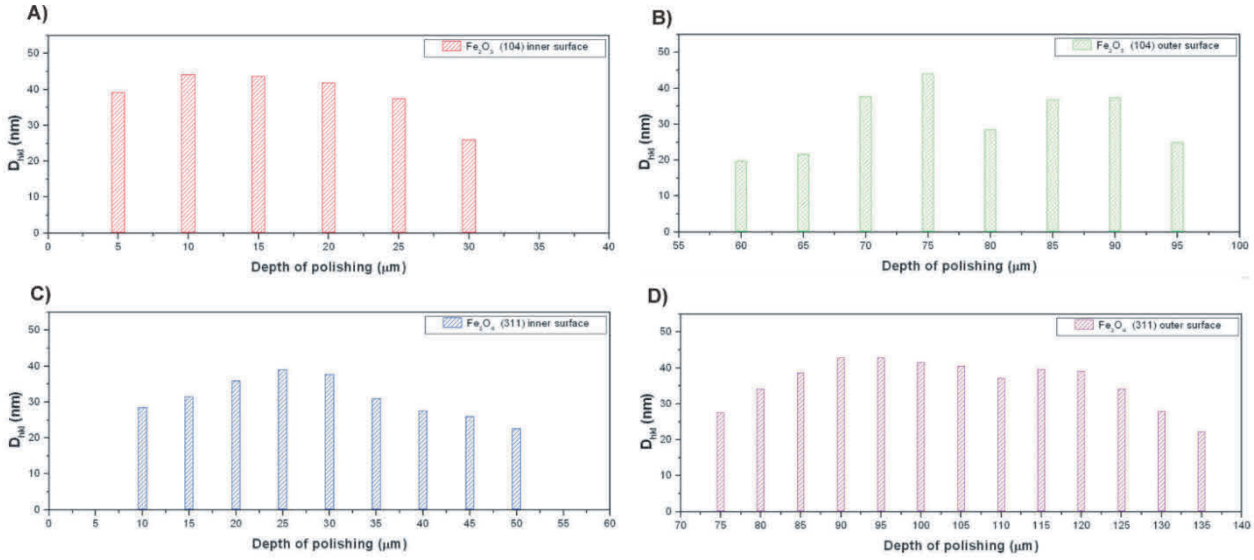

Figure 5 Determination of crystallite size D_{hkl} for main peaks Fe_3O_4 and Fe_2O_3: (a) hematite, the flowing steam side, (b) hematite, the flowing gas side, (c) magnetite, the flowing steam side, (d) magnetite, the flowing gas side

4. CONCLUSIONS

The obtained results of studies have shown that:

- oxide thickness more varies on the gas side but it is more uniform on the steam side. On the inside the oxide layer is composed of hematite and magnetite, while in the case of the tube wall outside also deposits exist apart from the aforementioned oxides,
- when comparing the results of structural examinations presented in paper [22] with D_{hkl} it is possible to state that greater degradation of the layer was observed for crystallites of larger sizes.
- The largest crystallite size for hematite was 44.20 nm and 46.23 nm for steam side and gas side, respectively. The largest crystallite size for magnetite was 39.08 nm and 43.01 nm for steam side and gas side, respectively.

REFERENCES

[1] SNOPIŃSKI P., TAŃSKI T., LABISZ K., RUSZ S., JONSTA P., KRÓL M. Wrought aluminium-magnesium alloys subjected to SPD processing. *International Journal of Materials Research*, 2016, vol. 107, no. 7, pp. 637-645.

[2] YIN K., QIU S., TANG R., ZHANG Q., ZHANG L. Corrosion behavior of ferritic/martensitic steel P92 in supercritical water. *The Journal of Supercritical Fluids*, 2009, vol. 50, pp. 235-239.

[3] SZAFARSKA M., IWASZKO J. Laser remelting treatment of plasma-sprayed Cr_2O_3 oxide coatings. *Archives of Metallurgy and Materials*, 2012, vol. 57, no. 1, pp. 215-221.

[4] KRUPIŃSKI M., KRUPIŃSKA B., RDZAWSKI Z., LABISZ K., TAŃSKI T. Additives and thermal treatment influence on microstructure of nonferrous alloys. *Journal of Thermal Analysis and Calorimetry*, 2015, vol. 120, pp. 1573-1583.

[5] GWOŹDZIK M., NITKIEWICZ Z. Topography of X39Cr13 steel surface after heat and surface treatment. *Optica Applicata*, 2009, vol. 39, no. 4, pp. 853-857.

[6] BANKIEWICZ D., ENESTAM S., YRJAS P., HUPA M. Experimental studies of Zn and Pb induced high temperature corrosion of two commercial boiler steels. *Fuel Processing Technology*, 2013, vol. 105, pp. 89-97.

[7] FRANGINI S., MASCI A., McPHAIL S. J., SOCCIO T., ZAZA F. Degradation behavior of a commercial 13Cr ferritic stainless steel (SS405) exposed to an ambient air atmosphere for IT-SOFC interconnect applications. *Materials Chemistry and Physics*, 2014, vol. 144, no. 3, pp. 491-497.

[8] VAKHGUELT A., KAPAYEVA S. D., BERGANDER M. J. Combination Non-Destructive Test (NDT) Method for Early Damage Detection and Condition Assessment of Boiler Tubes. *Procedia Engineering*, 2017, vol. 188, pp. 125-132.

[9] SUDIRO T., KYO S., ISHIBASHI O., NAKAMORI M., KUROKAWA K. High Temperature Corrosion of CoNiCrAlYSi Alloys in the Liquid Phase of Na_2SO_4-NaCl. *Materials Transactions*, 2012, vol. 53, no. 5, pp. 920-925.

[10] KIM Y. H., OAK J. J., BAE K. C., LEE W. J., PARK Y. H. High - temperature oxidation behavior and kinetics of forged 12Cr-MoVW steel. *Archives of Metallurgy and Materials*, 2017, vol. 62, no. 2B, pp. 1099−1104.

[11] ROJACZ H., BIRKELBACH F., WIDDER L., VARGA M. Scale adhesion, scratch and fracture behaviour of different oxides formed on iron based alloys at 700°C. *Wear*, 2017, vol. 380-381, pp. 126-136.

[12] LYTA, UEDA M., KAWAMURA K., TAKEYAMA M., MARUYAMA T. Microstructure Development of Oxide Scale during Steam Oxidation of the Fe20Cr30Ni2Nb (at. %) Austenitic Steel at 1073K. *Materials Transactions*, 2013, vol. 54, no. 12, pp. 2276-2284.

[13] GWOŹDZIK M., NITKIEWICZ Z. Texturing of magnetite forming during long-term operation of a pipeline of 10CrMo9-10 steel. *Solid State Phenomena*, 2013, vol. 203-204, pp. 121-124.

[14] ALMAZROUEE A. I., AL-FADHALAH K. J., ALHAJERI S. N., ALFEHAID S. High temperature corrosion of martensitic steel of re-heater pipes in a desalination power plant. *Engineering Failure Analysis,* 2018, vol. 85, pp. 89-96.

[15] GWOŹDZIK M., NITKIEWICZ Z. Analysis of crystallite size and lattice deformations changes in an oxide layer on P91 steel. *Archives of Metallurgy and Materials*, 2013, vol. 58, no. 1, pp. 31-34.

[16] GWOŹDZIK M. Analysis of crystallite size and lattice deformations changes in the oxide layer formed on steel operated for a long time at an elevated temperature. *Solid State Phenomena*, 2013, vol. 203-204, pp. 204-207.

[17] ISHITSUKA T., INOUE Y., OGAWA H. Effect of silicon on the steam oxidation resistance of a 9%Cr heat resistant steel. *Oxidation of Metals*, 2004, vol. 61, no. 1-2, pp. 125-142.

[18] GRUBER T., SCHARLER R., OBERNBERGER I. Application of an empirical model in CFD simulations to predict the local high temperature corrosion potential in biomass fired boilers. *Biomass and Bioenergy,* 2015, vol. 79, pp. 145-154.

[19] TALEKAR A., CHANDRA D., CHELLAPPA R., DAEMEN J., TAMURA N., KUNZ M. Oxidation kinetics of high strength low alloy steels at elevated temperatures. *Corrosion Science*, 2008, vol. 50, pp. 2804-2815.

[20] SANCHEZ L., HIERRO M. P., PEREZ F. J. Effect of chromium content on the oxidation behaviour of ferritic steels for applications in steam atmospheres at high temperatures. *Oxidation of Metals*, 2009, vol. 71, no. 3-4, pp. 173-186.

[21] GWOŹDZIK M. Analysis of crystallite size changes in an oxide layer formed on steel used in the power industry. *Acta Physica Polonica A*, 2016, vol. 130, no. 4, pp. 935-938.

[22] GWOŹDZIK M. Characterization of oxide layers formed on 13CrMo4-5 steel operated for a long time at an elevated temperature. *Archives of Metallurgy and Materials*, 2015, vol. 60, no. 3, pp. 1783-1788.

[23] PRISS J., ROJACZ H. KLEVTSOV I., DEDOV A., WINKELMANN H., BADISCH E. High temperature corrosion of boiler steels in hydrochloric atmosphere under oil shale ashes. *Corrosion Sciences*, 2014, vol. 82, pp. 36-44.

[24] NAKAI M., NAGAI K., MURATA Y., MORINAGA M. Improvement in steam oxidation resistance of Fe-10%Cr-0.08%C steel by suppressing. *Corrosion Science*, 2006, vol. 48, pp. 3869-3885.

[25] SRODA S., BAXTER D., ARPONEN M. The influence of alloying elements on the corrosion behaviour of ferritic steels in simulated combustion atmospheres. *Materials and Corrosion*, 2005, vol. 56, no. 11, pp. 791795.

[26] LAVERDE D., GOMEZ-ACEBO T., CASTRO F. Continuous and oxidation of T91 ferritic steel under steam. *Corrosion Science*, 2004, vol. 46, pp. 613-631.

[27] SUMIDA T., IKUNO T., OTSUKA N., SABURI T. High temperature oxidation behavior of 2.25%Cr-1%Mo steel boiler tubes in long-term exposure to superheated steam. *Materials Transactions, JIM*, 1995, vol. 36, no. 11, pp. 1372-1378.

[28] RETSCHITZEGGER S., GRUBER T., BRUNNER T., OBERNBERGER I. Short term online corrosion measurements in biomass fired boilers. Part 2: Investigation of the corrosion behavior of three selected superheater steels for two biomass fuels. *Fuel Processing Technology*, 2016, vol. 142, 59-70.

[29] EN 10028-2: Flat products made of steels for pressure purposes - Part 2: Non-alloy and alloy steels with specified elevated temperature properties.

[30] CULLITY B. D. *Podstawy dyfrakcji promieni rentgenowskich*. Warszawa: Państwowe Wydawnictwo Naukowe, 1964, p. 352-357.